

Effects of progressive oxygen depletion on sediment diagenesis and fluxes: A model for the lower St. Lawrence River Estuary

Sergei Katsev,¹ Gwénaëlle Chaillou, and Bjørn Sundby

Department of Earth and Planetary Sciences, McGill University, 3450 University Street, Montréal, Québec, H3A 2A7, Canada; Institut des Sciences de la Mer, Université du Québec à Rimouski, Rimouski, Québec, G5L 3A1, Canada

Alfonso Mucci

Department of Earth and Planetary Sciences, McGill University, 3450 University Street, Montréal, Québec, H3A 2A7, Canada

Abstract

We applied a diagenetic model to examine the effects of a decadal-timescale progressive decrease in bottom-water oxygen concentration on sediment geochemistry and fluxes across the sediment–water interface. The model was calibrated using geochemical data acquired over the last 30 yr in the lower St. Lawrence River Estuary (Canada), where the bottom-water oxygen concentration has been decreasing at an average rate of $1 \mu\text{mol L}^{-1} \text{yr}^{-1}$ over the past 70 yr. Benthic fluxes calculated from the model are comparable to fluxes derived from shipboard sediment incubations. By propagating the model forward in time and allowing the oxygen concentration to decrease further at $1 \mu\text{mol L}^{-1} \text{yr}^{-1}$, we predict changes in the distributions and fluxes of iron, manganese, phosphorus, nitrogen, and sulfur. As the oxygen concentration decreases, the concentrations and distributions of reactive phases in the sediment change at an accelerating pace. Fluxes of reduced substances out of the sediment increase, reactive iron and manganese oxide phases become depleted, and the sediment becomes progressively enriched in iron sulfides. A notable exception is the efflux of phosphate, which remains invariant. At the study site, these changes are likely to become measurable within the next 20 yr. Model results are sensitive to the effects of decreasing oxygen concentrations on the benthos, the response of which we represent by two different approximations of the bioturbation and bioirrigation formulations: a gradual decrease and a threshold-type decrease. The principal obstacle to reliable predictions of how sediments will respond is the lack of knowledge about the response of bioturbation and bioirrigation to decreasing oxygen in bottom waters.

The depth below the sediment–water interface where oxygen permeating from the water column is exhausted is known as the oxygen penetration depth (OPD). This depth separates environments dominated by aerobic and anaerobic metabolisms, and it reflects the balance between supply and consumption of oxygen. Variations in the flux of metabolizable organic matter to the sediment or in the concentration of oxygen in the bottom water can shift the location of the OPD and modify the distributions and fluxes of redox-sensitive elements (Gobeilet al. 1997; Kristensen 2000).

The effects of such variations are well documented for seasonal timescales (e.g., Aller 1994; Sayles et al. 1994; Thamdrup et al. 1994) and have been explored in several modeling studies (Soetaert et al. 1996; Berg et al. 2003; Morse and Eldridge 2007). In contrast, variations in the

supply and demand of oxygen over longer timescales have received less attention (Thomson et al. 1996; Jung et al. 1997; Burdige 2006). Katsev et al. (2006a) demonstrated that decadal variations in the flux of organic carbon to organic-poor sediments, such as in the deep basins of the Arctic Ocean, can shift the OPD by tens of centimeters and trigger a redistribution of redox-sensitive elements within the sediment column. Decadal-scale shifts in the OPD can also take place in fjords, landlocked basins, continental shelves adjacent to oxygen minimum zones, lakes undergoing eutrophication or remediation, and deep oceanic basins where bottom waters are replenished episodically.

The purpose of this paper is to examine the effects of decadal and longer-term trends in the bottom-water oxygen concentration on sediment geochemistry and fluxes across the sediment–water interface. To illustrate the response of sediments to such a trend, we apply a diagenetic model to the lower St. Lawrence River Estuary (LSLE), where the oxygen concentration in the bottom water has been declining at an average rate of $1 \mu\text{mol L}^{-1} \text{yr}^{-1}$ for the past 70 yr (Gilbert et al. 2005). The model is calibrated at steady state using geochemical data acquired over the last 30 yr and is propagated forward in time under a scenario of continuously decreasing oxygen concentrations until anoxia is reached. Model fluxes are compared to benthic fluxes measured with shipboard incubations during the past 10 yr, and changes in the distributions, speciations, and fluxes of diagenetically reactive elements (Fe, Mn, P, N, S) are

¹ Corresponding author (skatsev@d.umn.edu). Current address: Large Lakes Observatory and Department of Physics, University of Minnesota Duluth, 2205 E. 5th Street, Duluth, Minnesota 55812.

Acknowledgments

This research was funded by the Natural Sciences and Engineering Research Council of Canada (NSERC) through a postdoctoral fellowship to S.K. and a Strategic Project grant to B.S. and A.M. We thank the captain and the crew of R/V *Coriolis II* for their help during a cruise in August 2005, Stephanie Ringuet for technical assistance, as well as S. Dufour, M. Lehmann, and R. Aller for helpful discussions. We also thank Filip Meysman and an anonymous reviewer for their incisive comments.

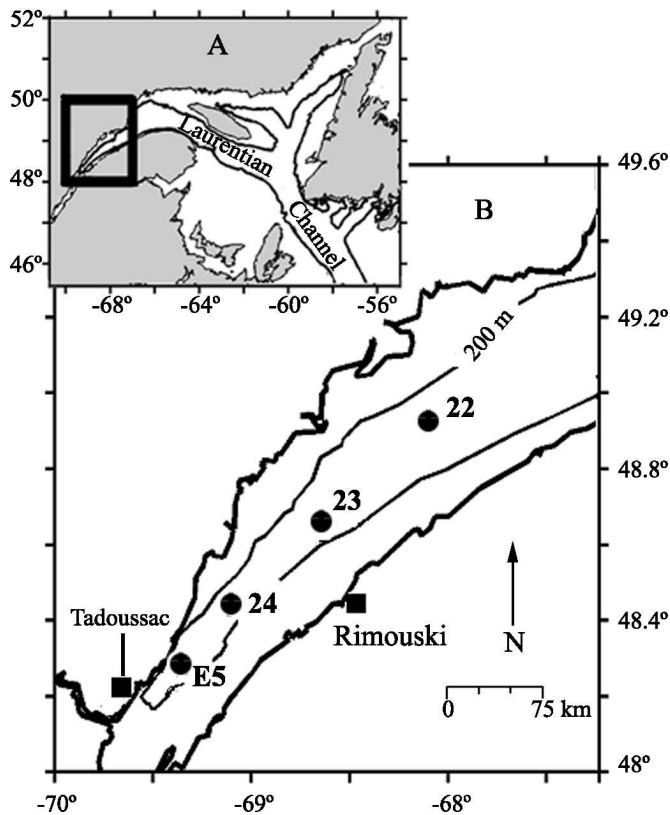


Fig. 1. (A) Gulf and Estuary of St. Lawrence with study area shown by outline. (B) Location of sampling sites in the Lower St. Lawrence River Estuary (circles).

predicted. Sensitivity analyses of calibrated (steady-state) and projected (transient) solutions identify the factors that most strongly affect sediment geochemistry.

Study area

The St. Lawrence River Estuary (Fig. 1) receives the discharge of one of the largest freshwater systems on the North American continent ($\sim 10,900 \text{ m}^3 \text{ s}^{-1}$; Bourgault and Koutitonsky 1999). The bathymetry of the estuary is dominated by the Laurentian Channel, a 250–500-m-deep submarine valley that extends landward 1,240 km from the edge of the continental shelf. The overall circulation pattern is estuarine; brackish water flows seaward in the surface layer, and water formed in the northwest Atlantic flows landward in the deep layer. The water in the deep layer is isolated from the atmosphere by a permanent pycnocline at 100–150-m depth. As it flows landward, the bottom water gradually loses oxygen through respiration and microbial degradation of organic matter settling through the water column. The time it takes for a parcel of water entering at the shelf edge to reach the head of the Laurentian Channel is estimated to be 3–4 yr (Gilbert et al. 2005). At depths greater than 150 m, oxygen consumed by respiration cannot be replenished by winter convection (Petrie et al. 1996). This makes oxygen concentration in the bottom water sensitive to the fluxes

of organic carbon and the rates of oxygen supply with the landward flow.

Dissolved oxygen in bottom waters—A compilation of historical measurements from 300–355-m depth in the LSLE shows that dissolved oxygen concentrations in the bottom water have decreased by more than 50% over the last 70 yr, from $130 \mu\text{mol L}^{-1}$ in the 1930s to about $60 \mu\text{mol L}^{-1}$ at present (Gilbert et al. 2005). One-half to two-thirds of the observed decrease has been attributed to a change in the oxygen content of the water that enters the Gulf of St. Lawrence from the Atlantic Ocean (Gilbert et al. 2005). The remaining oxygen depletion is likely caused by increased fluxes of organic matter to the seafloor (Benoit et al. 2006; Thibodeau et al. 2006). An area of about $1,300 \text{ km}^2$ of the Laurentian Trough is now bathed in hypoxic waters (Gilbert et al. 2005).

Sediments—The sediments that floor the estuary are silty clays with a thin oxidized surface layer and an organic carbon content of $\sim 2\%$ (dry weight). The oxygen concentration decreases sharply below the sediment–water interface and becomes undetectable at a depth varying between 0.2 and 1.0 cm, sometimes within the same core (Silverberg et al. 1987; Silverberg and Sundby 1990; Anschutz et al. 2000).

Despite the changing oxygen regime in the LSLE, no clear temporal trends have been identified in the distributions of redox-sensitive metals (Fe, Mn) and nutrients (N and P), neither in the sediment column, nor in fluxes across the sediment–water interface (Sundby et al. 1992; Silverberg et al. 1995, 2000; Anschutz et al. 1998, 2000). However, if the decreasing oxygen trend continues, at some point the sediment will be affected (Kristiansen et al. 2002; Sell and Morse 2006).

Fluxes across the sediment–water interface—To obtain data against which to test model results, a set of cylindrical sediment cores, 10-cm inner diameter and 50-cm length, were recovered in August 2005 at three locations (Stas. 22, 23, E5; Fig. 1) in the hypoxic zone of the LSLE using a Bowers & Connelly Multicorer (Barnett et al. 1984). Immediately upon recovery, two cores from each station were incubated in the dark for 60 h at 4°C as described by Hulth et al. (1994). A Plexiglas lid, equipped with a rubber O-ring, a magnetic stirring bar, and two Teflon valves for sampling, was fitted on the top of each core liner, leaving about 11 cm of ambient bottom water between the lid and the sediment surface. Care was taken to avoid trapping air bubbles under the lid. At regular intervals, 10-mL water samples were drawn into a glass syringe for oxygen analysis by the Winkler method. A second sample was collected with a plastic syringe and filtered through a Nalgene 0.2- μm cellulose acetate membrane filter. Aliquots of the filtrate were analyzed on board for nutrients, or acidified to pH 1.6 with ultrapure Seastar HNO_3 for later analysis of dissolved metals. The water removed during sampling was replaced by an equivalent volume of bottom water of known composition and oxygen concentration. The total amount of water withdrawn and replaced during each

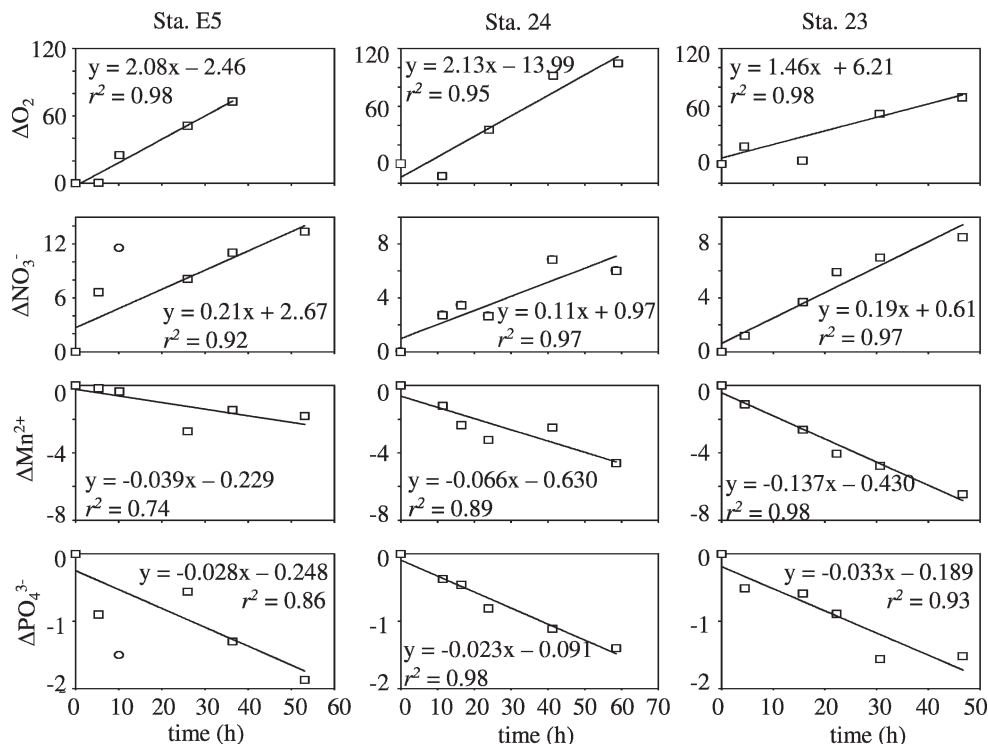


Fig. 2. Consumption (positive) or release (negative) of dissolved oxygen, nitrate, manganese, and phosphate in sediment incubation experiments. Plotted are changes in the respective concentrations ($\mu\text{mol L}^{-1}$) in the overlying water. Circles mark the data points that were excluded from calculations as outliers.

sample collection did not exceed 25% of the total volume of overlying water.

Soluble reactive phosphate (SRP) was determined immediately upon sampling by the spectrophotometric heptamolybdate method of Murphy and Riley (1962). Total dissolved nitrate ($\Sigma\text{NO}_3^- = \text{NO}_3^- + \text{NO}_2^-$) was analyzed within a few days on frozen aliquots using the flow-injection method of Anderson (1979). The detection limits were 0.8 and $0.5 \mu\text{mol L}^{-1}$ for SRP and nitrate, respectively, and the precision of both methods was $\pm 5\%$. Total dissolved Mn was determined in acidified water samples by flame atomic absorption spectrophotometry using external aqueous standard solutions for calibration. The detection limit was below $0.08 \mu\text{mol L}^{-1}$, and the precision was better than $\pm 5\%$. Dissolved Fe(II) was determined with the ferrozine procedure of Stookey (1970) with $\pm 5\%$ precision and a detection limit of $2 \mu\text{mol L}^{-1}$.

To correct for the composition of the replacement water, the change in concentration of a given element (ΔX) due to sediment–water exchange between samplings was calculated as:

$$\Delta X = [s_2] - \{((V_{\text{tot}} - V_{s1})[s_1] + V_{s1}[\text{refill}])/V_{\text{tot}}\} \quad (1)$$

where V_{tot} and V_{s1} are the total volume of overlying water and volume of water withdrawn in the previous sampling, respectively, whereas $[s_1]$, $[\text{refill}]$, and $[s_2]$ are, respectively, the concentrations of the element of interest in the previous sampling, in the replacement bottom water, and in the

current sampling. Concentration changes were plotted against time to derive an average rate of exchange across the sediment–water interface over the incubation period (Fig. 2). These rates, normalized to the surface area of the exposed interface (78.53 cm^2), were taken as a measure of the fluxes of oxygen, nitrate, phosphate, manganese, and iron across the sediment–water interface. The results are presented in Table 1.

The model

To simulate diagenesis of the LSLE sediments, we used the reaction-transport model LSSE-Mega, the numerical code of which is described in detail in Katsev et al. (2006a,b). Because model details, such as the number of reactive species and the values of kinetic constants, differ among model implementations, a detailed description is provided in the Web Appendix 1 to this paper (www.aslo.org/lo/toc/vol_52/issue_6/2555a1.pdf) and in the online database dSED (Katsev et al. 2004).

Several improvements were introduced in the present implementation: sediment compaction was considered explicitly (Meysman et al. 2005) using a measured porosity profile (see Web Appendix 1), and the bioirrigation formulation was modified to account for the difference in bioirrigation rates between oxidized and reduced solutes. The transport of solutes by the irrigation activities of burrow-dwelling organisms is typically described (e.g.,

Table 1. Fluxes ($\mu\text{mol cm}^{-2} \text{yr}^{-1}$) in (+) and out (-) of the sediment derived from sediment incubations and model simulations. Incubation results for Sta. 23 are bold, and this location corresponds to the geochemical profiles in Fig. 5. Both steady-state ($t = 0$) and transient (recorded at $t = 25$ yr) simulation results are presented. Transient simulations used $K_{D\text{bO}_2} = 50 \mu\text{mol L}^{-1}$ and $\varepsilon_{\text{Mn}} = \varepsilon_{\text{Fe}} = 0.6$. Simulation time $t = 25$ roughly corresponds to year 2005 under the approximation that the bottom-water O_2 concentration decreases from the reference state by $1 \mu\text{mol L}^{-1} \text{yr}^{-1}$.

	O_2	NO_3^-	Mn^{2+}	Fe^{2+}	H_3PO_4
Incubations					
Sta. E5	+234	+23.7	-4.4	(-) <2.5	-3.3
Sta. 24	+237	+15.3	-6.9	(-) <2.5	-2.6
Sta. 23	+157*	+20.8	-15.3	(-) <2.5	-3.6
Model at ref. state ($t=0$)	+150	+20.4	-10.2	-0.73	-2.2
Model at $t=25$ yr	+120	+22.63	-13.1	-1.10	-2.2
Contribution of bioirrigation to total flux in reference state	40%	87%	99%	95%	43%

* Best estimate (sample appeared to be contaminated by an air bubble).

Meile et al. 2005) as proportional to $\alpha_{\text{irr}}(C_i^0 - C_i)$, where C_i and C_i^0 are the concentrations of solute i in the sediment pore water and water overlying the sediment, respectively, and α_{irr} describes the intensity of bioirrigation. Because reduced solutes are consumed or precipitated at the oxidized burrow wall, they barely penetrate into the burrow water. Hence, they effectively experience lower bioirrigation rates than oxidized species (Meile et al. 2005). In some studies (e.g., Berg et al. 2003), this effect was accounted for by introducing a correction factor for the bioirrigation coefficient α_{irr} . However, since this coefficient characterizes the activity of irrigating organisms, it should be solute independent, and it is more appropriate to correct the solute concentration in the burrow rather than the bioirrigation coefficient. We therefore introduce the term $\alpha_{\text{irr}}(C_i^0 - C_i^{\text{bur}})$, where C_i^{bur} is the concentration of a species in the water of a bioirrigated burrow. The two approaches produce similar results when the concentration of solute in the overlying water, C_i^0 , is small, which is typically the case for reduced species. We obtain the concentration C_i^{bur} for Fe(II), Mn(II), NH_4^+ , and H_2S , as well as for P, which adsorbs on the oxidized iron that lines burrow walls, by multiplying the pore-water concentration C_i by a factor of 0.1. For other species, we use $C_i^{\text{bur}} = C_i$.

Transient simulations require several additional modifications to the sediment model. One is to couple influxes and effluxes of elements at the sediment surface to account for their transformations in the overlying water column (Soetaert et al. 2000). Such coupling can potentially generate positive feedbacks that strongly influence transient diagenetic regimes (Katsev et al. 2006b). In the present case, it can affect the sedimentation fluxes of Mn and Fe oxides. Another modification is related to the response of bioturbation and bioirrigation to decreasing oxygen levels. These modifications are described next.

Coupling between sediment and water column—Solute released from the sediment can generate particulate phases—by reoxidation, precipitation, adsorption, or incorporation into organic particles—and become redeposited into the sediment. This creates a coupling between elemental influxes and effluxes. We characterize this coupling for iron and manganese by introducing the

recycling coefficients ε_{Fe} and ε_{Mn} . These are defined as $\Phi_{\text{rec},i}/\Phi_{\text{out},i}$, where $\Phi_{\text{out},i}$ is the molar flux of the element i out of the sediment and $\Phi_{\text{rec},i}$ is the fraction of that flux that returns to the sediment (Fig. 3). Specifically, an efflux of Fe^{2+} , $\Phi_{\text{out,Fe}}$, generates a “recycled” sedimentation flux of ferric iron, $\varepsilon_{\text{Fe}}\Phi_{\text{out,Fe}}$, that contributes to the total sedimentation flux of ferric iron, $F_{\text{Fe}(\text{OH})_3}$. Likewise, the flux of Mn^{2+} from the sediment contributes to the sedimentation flux, F_{MnO_2} , of manganese oxide. The “nonrecycled” part of the efflux, $(1 - \varepsilon_i)\Phi_{\text{out},i}$, is assumed to be flushed from the system or immobilized within refractory compounds. The relationship between the total sedimentation flux $\Phi_{\text{sed},i}$, as measured for example by sediment traps, and the net external input $\Phi_{\text{ext},i}$, such as from terrestrial or upstream sources, is given by $\Phi_{\text{sed},i} = \Phi_{\text{ext},i} + \Phi_{\text{rec},i} = \Phi_{\text{ext},i} + \varepsilon_i\Phi_{\text{out},i}$. In steady-state simulations,

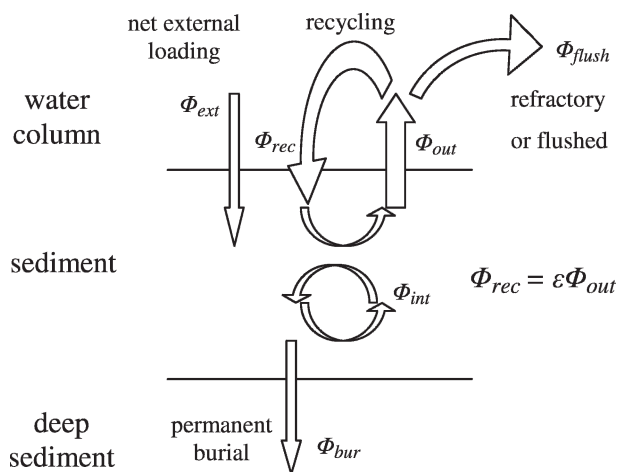


Fig. 3. Recycling of sedimentary constituents in the water column. Substances released from the sediment (flux Φ_{out}) are redeposited in one form or another (Φ_{rec}) or removed from the system (Φ_{flush}). The molar redeposition flux is $\Phi_{\text{rec}} = \varepsilon\Phi_{\text{out}}$, where ε is the efficiency of recycling and values vary between 0 and 1. The total flux of material reaching the sediment surface is $\Phi_{\text{sed}} = \Phi_{\text{rec}} + \Phi_{\text{ext}}$, where Φ_{ext} is the net sedimentation flux from external sources. Φ_{bur} is the burial flux into the deep sediment. Φ_{int} represents mass fluxes within the diagenetically active layer of the sediment column.

only the total flux $\Phi_{\text{sed},i}$ needs to be specified at the model boundary, in which case the solutions become independent of the recycling efficiency. In transient simulations, total sedimentation fluxes of Mn and Fe oxides at the model boundary, $F_{\text{MnO}_2} = \Phi_{\text{sed},\text{Mn}}$ and $F_{\text{Fe(OH)}_3} = \Phi_{\text{sed},\text{Fe}}$, respectively, were calculated for constant (specified) recycling coefficients, ε_{Mn} and ε_{Fe} , and fixed external inputs, $\Phi_{\text{ext},\text{Mn}}$ and $\Phi_{\text{ext},\text{Fe}}$. The external inputs were calculated at the start of each transient simulation run as $\Phi_{\text{ext},i} = \Phi_{\text{sed},j}^{\text{st}} - \varepsilon_i \Phi_{\text{out},j}^{\text{st}}$, where $\Phi_{\text{sed},j}^{\text{st}}$ is the total sedimentation flux at the initial (reference) state. The initial flux out of the sediment, $\Phi_{\text{out},j}^{\text{st}}$, was calculated from model concentration gradients at the reference state (Table 1). During the course of the transient simulations, the fluxes $\Phi_{\text{out},j}^{\text{st}}$ were recalculated at each iteration step.

Relative to the decadal timescale of interest in this study, recycling of Fe(II) and Mn(II) in the water column is fast. In seawater, reduced iron is typically oxidized on timescales of minutes to hours (Millero et al. 1987), and reduced manganese is oxidized on timescales of hours in the presence of MnO_2 , carbonate particles, or bacteria (Morgan 2005). Accordingly, we adopted a “reflective” boundary condition (Soetaert et al. 2000) for both iron and manganese, i.e., with no explicit time delay between release and redeposition.

Response of bioturbation and bioirrigation to decreasing oxygen concentrations—During intermittent hypoxic events, oxyconforming benthic species respond to low oxygen concentrations by slowing down their activities and lowering their oxygen requirements. Others (oxyregulators) maintain relatively fixed metabolic rates and respond by increasing the rate of burrow ventilation (Forster et al. 1995; Kristensen 2000). In the long term, diminishing availability of oxygen reduces biomass, diversity, and abundance, and modifies the composition of the benthic community (Ritter and Montagna 1999).

Quantitative descriptions of the effects of diminishing oxygen concentration on sediment bioturbation and bioirrigation are rare. Expressions used for the relationship between the bioturbation coefficient, D_b , and the oxygen concentration at the sediment-water interface, $[\text{O}_2]^0$, range from linear (Fossing et al. 2004; Morse and Eldridge 2007) to strongly nonlinear (Ritter and Montagna 1999). We consider two types of functional dependencies. In the first type (Fig. 4), the biodiffusion coefficient at the sediment surface, D_b^0 , decreases with $[\text{O}_2]^0$ according to:

$$D_b^0 = D_{b,\text{ref}}^0 (1 - \eta) \frac{K_{D_b\text{O}_2} + [\text{O}_2^{\text{ref}}]}{[\text{O}_2^{\text{ref}}]} \frac{[\text{O}_2]^0}{K_{D_b\text{O}_2} + [\text{O}_2]^0} + \eta D_{b,\text{ref}}^0 \quad (2)$$

where $[\text{O}_2^{\text{ref}}]$ is a reference concentration of oxygen (set at $80 \mu\text{mol L}^{-1}$ for the LSLE), $D_{b,\text{ref}}^0$ is the bioturbation coefficient at $[\text{O}_2^{\text{ref}}]$, and $K_{D_b\text{O}_2}$ is a characteristic oxygen concentration at which D_b^0 decreases by a factor of 2. The dimensionless parameter η represents the residual bioturbation in a fully anoxic sediment.

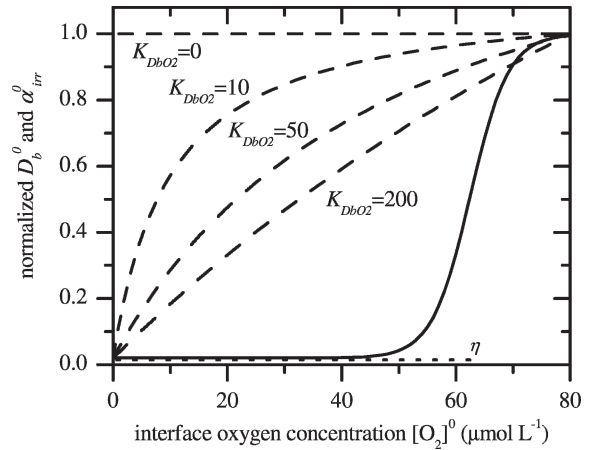


Fig. 4. The dependence of bioturbation (D_b^0) and bioirrigation (α_{irr}^0) coefficients on oxygen concentration $[\text{O}_2]^0$ at the sediment–water interface. The coefficients are normalized to their respective values at the reference oxygen concentration $[\text{O}_2]^0_{\text{ref}} = 80 \mu\text{mol L}^{-1}$. The parameter $K_{D_b\text{O}_2}$ (in $\mu\text{mol L}^{-1}$) is defined in Eq. 2. The solid line corresponds to the scenario where benthic activity decreases sharply at the hypoxic threshold (Eq. 3); η is the residual bioturbation or bioirrigation activity in a fully anoxic sediment.

The second approximation (Fig. 4) assumes that D_b^0 decreases sharply within a relatively narrow range of $[\text{O}_2]^0$ concentrations around a threshold value:

$$D_b^0 = D_{b,\text{ref}}^0 (1 - \eta) \frac{1}{1 + \exp(-\tau([\text{O}_2]^0 - [\text{O}_2]^{\text{thr}}))} + \eta D_{b,\text{ref}}^0 \quad (3)$$

Here, $[\text{O}_2]^{\text{thr}} = 62.5 \mu\text{mol L}^{-1}$ is the threshold concentration that corresponds to severe hypoxia (Diaz and Rosenberg 1995). The coefficient τ characterizes the steepness of the D_b^0 vs. $[\text{O}_2]^0$ curve. In the absence of more information, we chose $\tau = 0.3 \mu\text{mol L}^{-1}$ and $\eta = 0.02$. The bioirrigation coefficient at the sediment–water interface, α_{irr}^0 , is considered to have the same functional dependence on $[\text{O}_2]^0$ as D_b^0 (Eqs. 2 and 3).

Computed Axial Tomography (CAT) scan images of sediment cores collected in August 2005 suggest that the response of bioturbation to decreasing oxygen concentration is better described by a threshold-type approximation such as Eq. 3 (S. Dufour pers. comm.). These images show abundant deep burrows at several stations in the LSLE. At Stas. 22 and 24 (Fig. 1), where the levels of O_2 in the bottom water in August 2005 were 80 and $70 \mu\text{mol L}^{-1}$, respectively, the burrows connect to the sediment surface. At Sta. 23, where the oxygen concentration was below $60 \mu\text{mol L}^{-1}$, most burrows appear to end about 2 cm below the sediment surface, suggesting that the original burrows were abandoned by their inhabitants. If the 2-cm depth horizon reflects the timing of the abandonment (or mortality), a local sedimentation rate of $\sim 0.5 \text{ cm yr}^{-1}$ (Thibodeau et al. 2006) suggests that the burrows were abandoned approximately four years previously. A further

indication of the rapid shift in bioturbation regime is a recent invasion by Capitellid worms at Sta. 23 (P. Archambault pers. comm.). These worms, which irrigate the sediment to a depth of about 2 cm, are typically found in highly stressed (e.g., organic-rich, ammonia-rich) environments (Rosenberg 2001).

Numerical modeling and calibration at steady state—To calibrate the model for the conditions observed in the LSLE, we used site specific parameters such as sedimentation rate, bioturbation rate, etc., for an extensively sampled site situated in the middle of the LSLE (Sta. 23; Silverberg and Sundby 1990) (Fig. 1). The dissolved oxygen concentration at the sediment–water interface was assigned a value of $80 \mu\text{mol L}^{-1}$, which corresponds to the conditions in the LSLE in the late 1970s and early 1980s (Gilbert et al. 2005). Vertical distributions of dissolved and solid-phase species observed at this site between 1977 and 2005 are compiled in Fig. 5. Few data are available before 1977. The profiles show no apparent temporal trends. The amounts of extractable reactive Mn and Fe oxides appear to have decreased since 1980s, but the extraction techniques used in different years were not identical. In addition, the solid-phase and pore-water profiles are likely affected by spatial variability within the same location (Lavigne et al. 1997) and by temporal variations caused by seasonally variable organic matter fluxes to the seafloor.

The model was tuned via a sequential procedure whereby model parameters (the flux of organic carbon to the sediment surface, organic carbon reactivity, etc.) were adjusted until the model solutions approached the observed field data. The steady-state solution is shown in Fig. 5. The depth of oxygen penetration in the simulated reference state is deeper than the most recently measured one (0.4 cm), which is consistent with the trend of decreasing oxygen concentration in the bottom water. Discrepancies among simulated and measured species distributions are attributed to spatial heterogeneity, temporal variability (see following), absence of a diffusive boundary layer in the model formulation, the operational nature of the chemical extractions used to determine the concentrations of solid phases, variations between the extraction methods used in different years, and inherent uncertainties in model parameters.

Numerical modeling and simulations of transient states—To simulate the response of the sediment to a progressive depletion in bottom-water oxygen, the model was propagated forward for 80 yr from the reference steady state. A time-dependent boundary condition was imposed whereby the oxygen concentration at the sediment–water interface, $[\text{O}_2]^0$, decreased at a constant rate of $1 \mu\text{mol L}^{-1} \text{yr}^{-1}$, which is the average rate of oxygen depletion in the bottom waters of the LSLE over the past 70 yr (Gilbert et al. 2005). All other model parameters, with the exception of those for bioturbation and bioirrigation (see previous), were kept constant. Since the bottom-water oxygen concentration in the reference state ($80 \mu\text{mol L}^{-1}$) corresponds to the early 1980s, the time $t = 20\text{--}25$ ($[\text{O}_2]^0 = 55\text{--}60 \mu\text{mol L}^{-1}$) in our simulations corresponds to the early to mid-2000s. The

simulated time interval thus includes two decades before present, plus 60 yr into the future.

To examine the effects of uncertainties in model parameterization on the dynamics of benthic fluxes, the model was run 50 times for different combinations of model parameters. To vary the parameters simultaneously, a Halton randomization sequence (Reichert et al. 2002) was employed to generate parameter values; the model parameters were thus evenly sampled within the specified ranges (see Web Appendix 1).

The recycling coefficients ε_{Fe} and ε_{Mn} cannot be derived from sediment data and are therefore treated as adjustable parameters. Nevertheless, their magnitudes can be estimated from other considerations. Sundby and Silverberg (1985) estimated that approximately 40% of the Mn released from the sediment in the St. Lawrence River Estuary is flushed to the open ocean, which corresponds to a recycling coefficient ε_{Mn} of ~ 0.6 . In view of the similar geochemical reactivity of reduced and oxidized iron and manganese in the water column, the recycling coefficient for iron, ε_{Fe} , is likely to be comparable to ε_{Mn} .

We did not consider the recycling of the nutrients P and N. These elements are recycled in the water column chiefly by primary production in the photic zone. The fluxes of P and N out of the sediment, however, are negligible compared to the P and N inputs by the St. Lawrence River and the upwelling water at the head of the Laurentian Channel (Yeats 1988). A historical compilation of nutrient data over the past 35 yr shows that N and P concentrations have not varied appreciably in the deep water of the St. Lawrence River Estuary (D. Gilbert pers. comm.).

Results and discussion

Measured vs. predicted fluxes—The fluxes of dissolved iron, manganese, nitrate, phosphate, and oxygen calculated at reference steady state are well within a factor of two of the fluxes measured with shipboard incubations of cores at Sta. 23 (Table 1). The flux calculations account for solute transport by molecular diffusion, bioturbation, and bioirrigation. The calculated Fe flux is below the detection limit of the incubation method, and no flux of dissolved iron was detected during the incubations. The calculated oxygen fluxes are within the range of $98\text{--}420 \mu\text{mol cm}^{-2} \text{yr}^{-1}$ measured at Sta. 23 by Silverberg et al. (1995) and in good agreement with the value of $128 \mu\text{mol cm}^{-2} \text{yr}^{-1}$ obtained by the same authors in mesocosm experiments with sediments recovered from Sta. 23.

Figure 6 presents the model parameters that most affect the fluxes of oxygen, nitrate, iron, manganese, and phosphorus across the sediment–water interface. The sensitivity analysis was carried out by comparing the values of fluxes at the reference steady state with those obtained at steady state by changing individual model parameters by 10%. A complete list of the parameters used in the sensitivity analysis can be found in Web Appendix 1.

Sediment diagenesis at the reference steady state—At a bottom-water oxygen concentration $[\text{O}_2]^0 =$

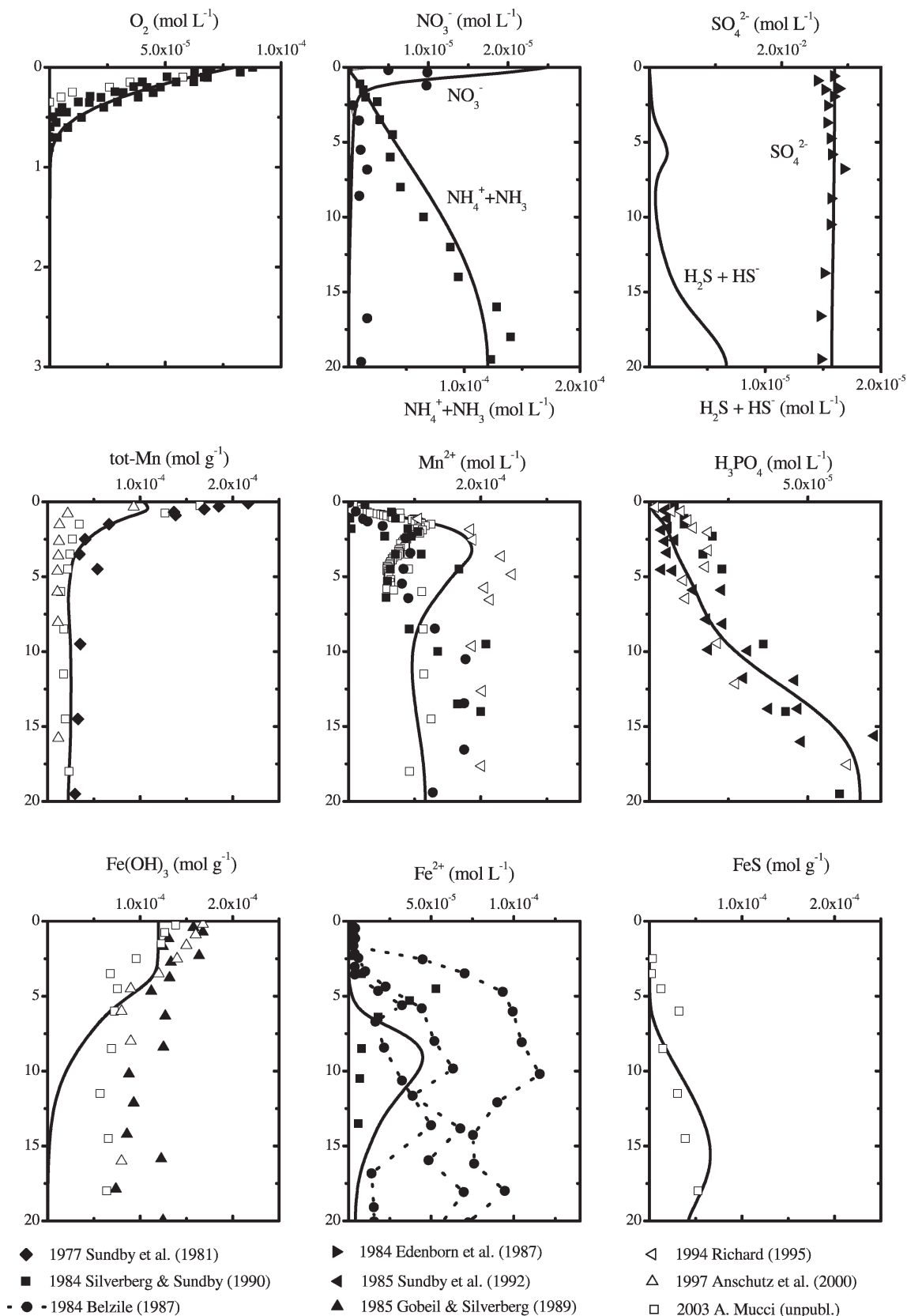


Fig. 5. Model calibrated to the geochemical data at Sta. 23. Filled symbols correspond to data collected between 1977 and 1990; open symbols correspond to data collected between 1991 and 2005. The years of the respective sample collections are indicated in the symbol legend. Solid lines are the calculated profiles at the reference steady state. Note that species distributions are affected by changes in the sediment redox conditions and steady-state profiles may not always adequately match the measurements. Simulated transient profiles for different times (*t*) are shown in Fig. 11.

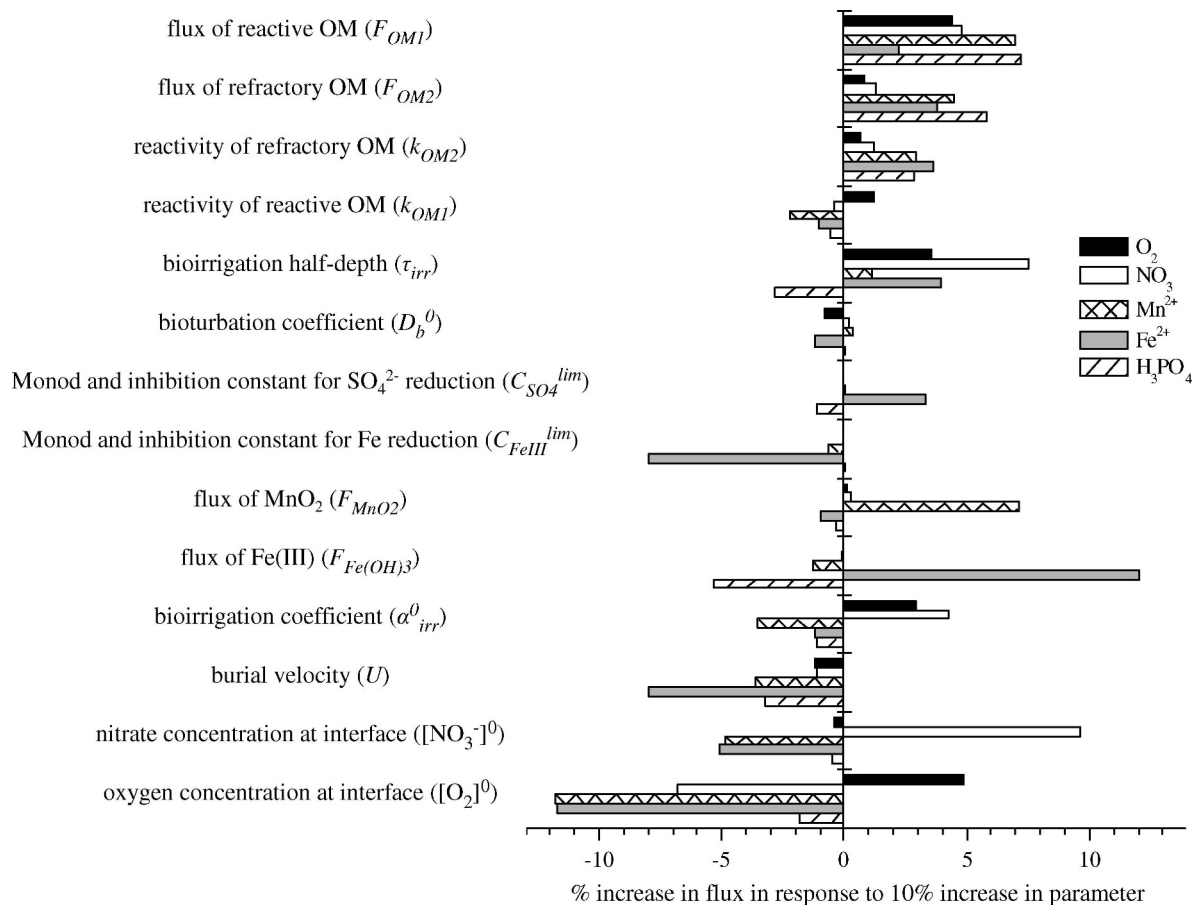


Fig. 6. Variations (%) of the steady-state fluxes of O₂, NO₃⁻, Mn²⁺, Fe²⁺, and H₃PO₄ in response to a 10% increase in selected model parameters relative to the reference steady-state values.

80 $\mu\text{mol L}^{-1}$, the oxygen penetration depth is simulated at ~ 0.7 cm (Fig. 5). With this relatively thin oxic layer, redox-sensitive elements, such as Mn and Fe, cycle close to the sediment–water interface. Manganese and iron oxides undergo reductive dissolution down to 3-cm and 10-cm depths, respectively. Most of the upward flux of Mn(II) and a large proportion of the Fe(II) flux are oxidized and precipitated in the oxic layer. A substantial fraction of Fe(II) is also immobilized within the sediment as iron sulfides, which accumulate below 5-cm depth. The upward transport of Mn(II) and the downward transport of oxidants (O₂ and NO₃⁻) by bioirrigation result in a trough in the dissolved Mn(II) profile (Fig. 5). Although chemically extractable Fe is present below the 10-cm depth (Fig. 5), significant sulfate reduction in these sediments (Edenborn et al. 1987), which is energetically less favorable than iron reduction, suggests that only a fraction of the extracted iron is available for reduction (Anschutz et al. 2000; Larsen et al. 2006). Accordingly, the [Fe(OH)₃] variable in our simulations corresponds only to the available fraction.

Nonlocal transport by bioirrigation is an important contributor to the total flux of oxidized solutes (Glud et al. 1994). For instance, the diffusive flux of NO₃⁻ into the sediment, as estimated from measured and modeled concentration gradients at the sediment–water interface

(Fig. 5) using Fick's first law, measured porosity, and the molecular diffusion coefficient for nitrate, is much smaller than the modeled and measured fluxes of total nitrate (Table 1). This disparity between the diffusive and total fluxes has also been noted at the same study location by others (M. Lehmann pers. comm.).

The integrated rate of oxic respiration over the length of the core, R_{O_2} , suggests that as much as 30% of the organic carbon flux is mineralized by oxic respiration despite the shallow penetration of oxygen. The reason for this is that a large fraction (about 30% in the model) of the deposited organic matter is sufficiently reactive that it decomposes before it can be buried deeper into the sediment. The model partitions the remaining mineralization among anaerobic respiration pathways as follows: 2% denitrification, 24% Mn reduction, 9% Fe reduction, 26% sulfate reduction, and 9% methanogenesis. The estimated rate of sulfate reduction is consistent with the value (26%) derived for Sta. 23 by Edenborn et al. (1987) based on a core recovered in 1983.

At the reference state, the molar ratios of manganese and iron effluxes to their respective deposition fluxes ($\Phi_{out} : \Phi_{sed}$ in Fig. 3) are, respectively, 0.76 and 0.03 (Fig. 7). The fraction of sedimentary Fe released to the water column is lower than that for Mn because Fe is cycling deeper in the sediment and is immobilized within the sediment column. The simulated vertical distributions of solid-iron phases

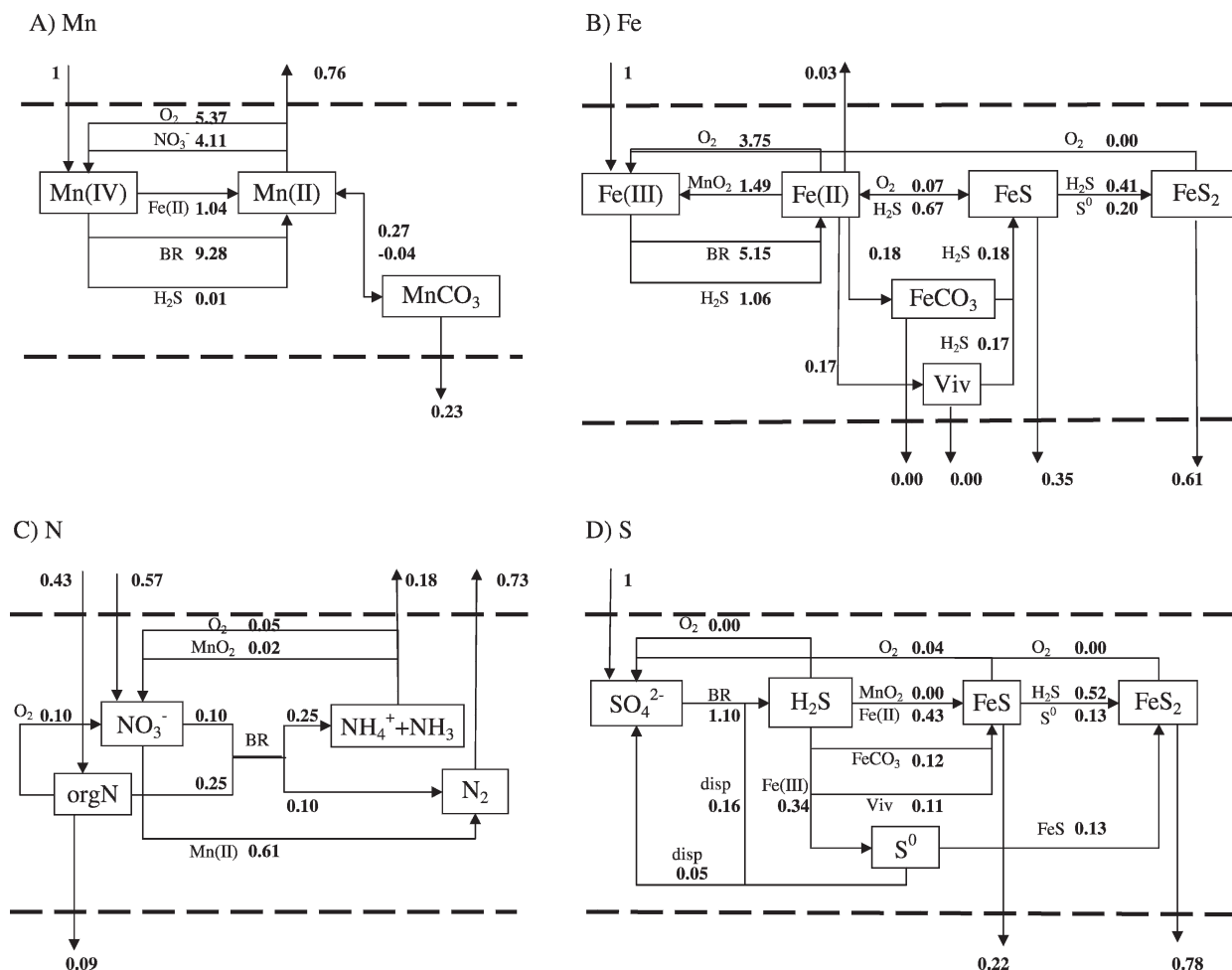


Fig. 7. Simulated cycling of (A) Mn, (B) Fe, (C) N, and (D) S in the sediment at the reference steady state (Fig. 5). Individual pathways correspond to model reactions described in the electronic supplements. Numbers are the integrated rates of the respective processes, normalized to the total input of a given element. Values above and below the dashed lines correspond to the sediment–water exchanges and burial fluxes, respectively. Pathway labels correspond to the redox couples in the respective processes. BR = bacterial reduction coupled to organic matter oxidation, disp = sulfur disproportionation, Viv = vivianite. The species marked on the diagram correspond to the model variables. Note that such model species as FeCO_3 and vivianite may not necessarily represent those exact minerals but are effective representations of phases with analogous behaviors.

suggest that iron is buried primarily as solid sulfides (FeS_x : acid volatile sulfides and pyrite), whereas most of the manganese (76%) is returned to the water column by diffusion and bioirrigation. According to the model, a small amount of solid Mn is buried with carbonates or adsorbed to other sediment solids. This compares favorably with the results of Sundby and Silverberg (1985), who estimated the fraction of Mn released to the overlying waters to be 82%.

Transient-state simulations—If the organic carbon flux is fixed, the oxygen penetration into the sediment decreases with decreasing oxygen concentration in the overlying water (Fig. 8). As long as the oxygen concentration is high enough that oxic respiration within the oxic layer dominates over other pathways of organic carbon mineralization (in the model formulation, this occurs as long as $[\text{O}_2]^0$ is larger than the Monod constant $C_{\text{O}_2}^{\text{lim}}$), the OPD decreases almost linearly with decreasing $[\text{O}_2]^0$. At lower oxygen concentrations, the simple linear relationship

breaks down, and the migration of the OPD toward the sediment–water interface accelerates slightly (Epping and Helder 1997). The linear relationship between the OPD and $[\text{O}_2]^0$ is in agreement with an analytical expression derived by Revsbech et al. (1980) approximating a constant oxygen consumption rate and is typical for organic-rich sediments. In organic-poor sediments, the relationship can become strongly nonlinear (Katsev et al. 2006a).

Figure 9 illustrates the effect of decreasing oxygen concentrations on mineralization pathways of organic matter. As the oxygen concentration at the interface decreases, anaerobic respiration gradually replaces aerobic respiration. The rates of iron and manganese reduction, which are limited by the amounts of the respective metal oxides, also decrease at low oxygen concentrations because the pools of both Fe and Mn oxides become depleted via loss to the water column and conversion to reduced solid phases. At oxygen concentrations below $20 \mu\text{mol L}^{-1}$, most of the sedimentary organic matter is mineralized by

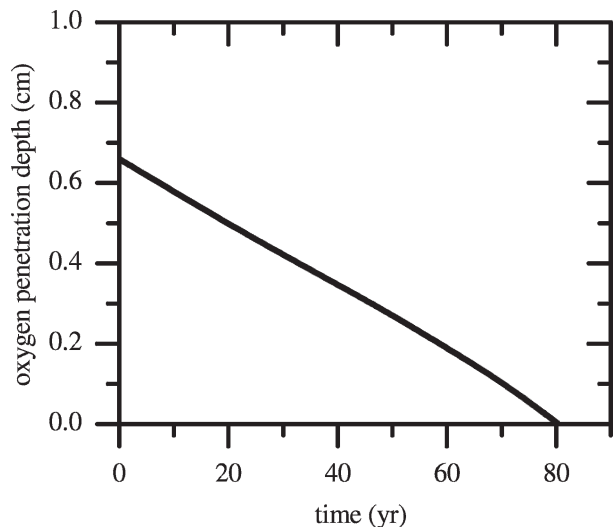


Fig. 8. Variations of the sediment oxygen penetration depth (OPD) as the O_2 concentration at the sediment–water interface is decreased from the reference state at the rate of $1 \mu\text{mol L}^{-1} \text{yr}^{-1}$. $\varepsilon_{\text{Fe}} = \varepsilon_{\text{Mn}} = 0.6$, $K_{\text{DbO}_2} = 50 \mu\text{mol L}^{-1}$.

the reduction of sulfate, which can be readily replenished by diffusion from the overlying water.

Fluxes across the sediment–water interface—Figure 10 presents model predictions of oxygen, nitrate, Mn(II), Fe(II), and phosphate fluxes across the sediment–water interface over the 80 yr that lead to anoxia. The figure shows the range of solutions obtained for 50 randomized combinations of model parameters (see Fig. 10 caption and Web Appendix 1). The randomized parameters include those identified as significant by the steady-state sensitivity analysis in Fig. 6, as well as the recycling coefficients ε_{Fe} and ε_{Mn} , and K_{DbO_2} .

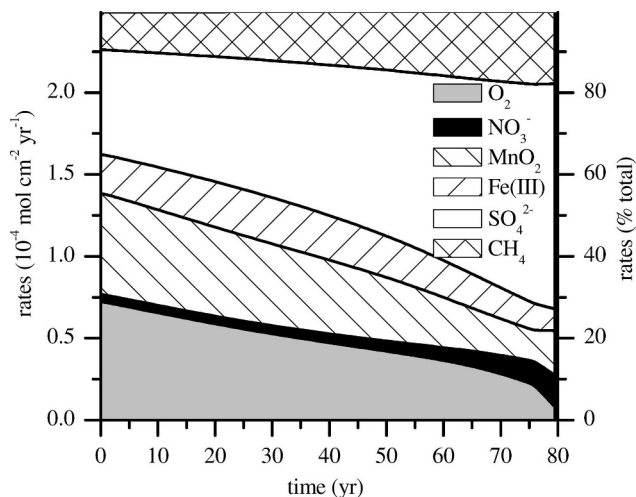


Fig. 9. Variations of the rates of organic-matter mineralization processes as the O_2 concentration at the sediment–water interface is decreased from the reference state (Fig. 5) at the rate of $1 \mu\text{mol L}^{-1} \text{yr}^{-1}$. The rates were calculated by integrating the rates of individual organic matter degradation pathways over the top 20 cm of sediment. $\varepsilon_{\text{Fe}} = \varepsilon_{\text{Mn}} = 0.6$, $K_{\text{DbO}_2} = 50 \mu\text{mol L}^{-1}$.

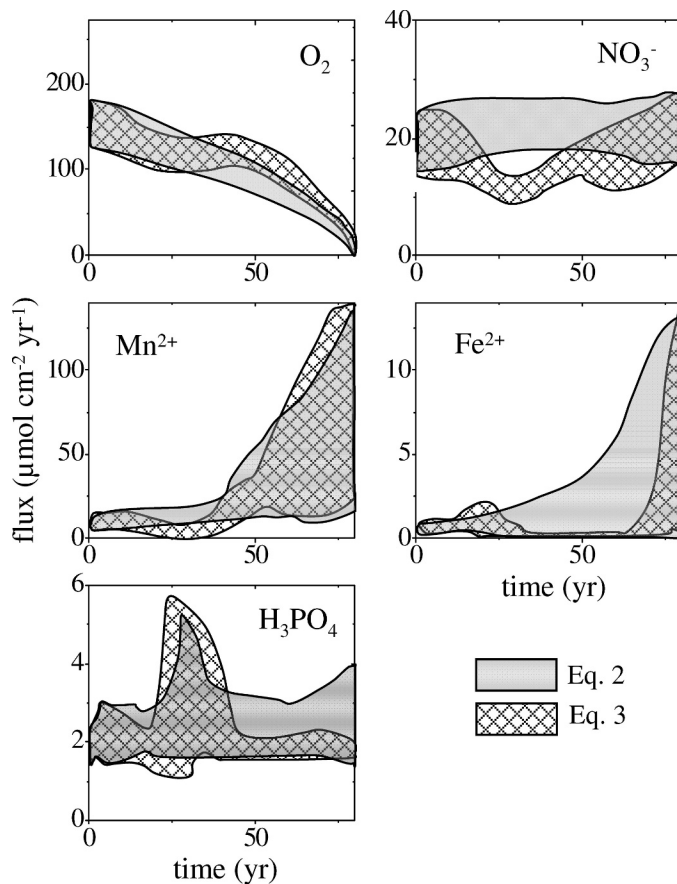


Fig. 10. Simulated temporal variations in the absolute values of benthic fluxes as the O_2 concentration at the sediment–water interface is decreased at the rate of $1 \mu\text{mol L}^{-1} \text{yr}^{-1}$. The outlines represent the ranges of solutions corresponding to 50 randomized combinations of model parameters. The randomized parameters included those identified in the steady-state sensitivity analysis in Fig. 6 (varied within a $\pm 20\%$ range), K_{DbO_2} (varied between 0 and $100 \mu\text{mol L}^{-1}$), and ε_{Mn} and ε_{Fe} (varied between 0 and 1). For a complete list, see Web Appendix 1. Simulation time is counted from the calibration conditions characterized by $[O_2]^0 = 80 \mu\text{mol L}^{-1}$. Two sets of simulations correspond to different approximations (Eqs. 2 and 3) for the response of bioturbation and bioirrigation to decreasing oxygen concentrations.

The flux of oxygen into the sediment decreases with diminishing oxygen availability (Fig. 10). As the oxic sediment layer becomes thinner, the oxidized solid species, such as Mn and Fe oxides, become exposed to reducing conditions in the presence of reactive organic matter progressively closer to the sediment surface. The pore-water Fe(II) and Mn(II) concentrations increase below the oxic–anoxic interface, their gradients become steeper, and the fluxes of Fe(II) and Mn(II) across the sediment–water interface increase accordingly.

Although the uncertainty in the projected solutions is significant (Fig. 10), for both formulations of the bioturbation/bioirrigation parameters (Eqs. 2 and 3), the upward fluxes of dissolved Mn(II) and Fe(II) generally increase with time, and the rate of change accelerates as anoxia is approached. The solutions with high Mn and Fe fluxes

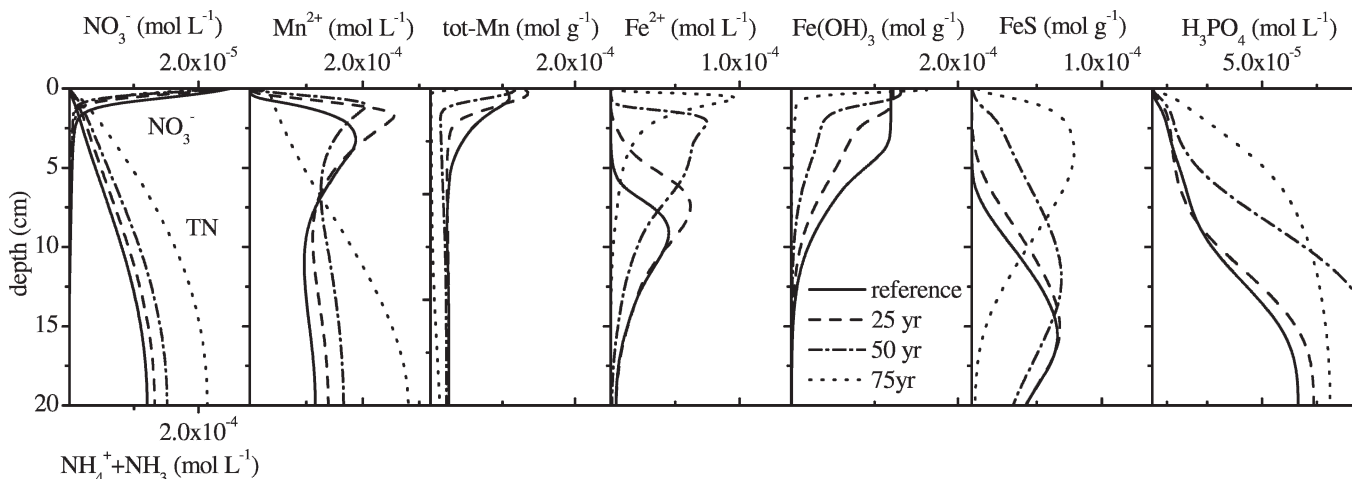


Fig. 11. Evolution of sediment composition as the O_2 concentration at the sediment–water interface decreases at the rate of $1 \mu\text{mol L}^{-1} \text{yr}^{-1}$ from the reference steady state (solid line): at $t = 25$ yr (dash), 50 yr (dash-dot), and 75 yr (dot). $\epsilon_{\text{Mn}} = \epsilon_{\text{Fe}} = 0.6$; $K_{\text{DbO}_2} = 50 \mu\text{mol L}^{-1}$. Concentration units are mol cm^{-3} for solutes and mol g^{-1} for solids.

generally correspond to the larger values of α_{irr}^0 , whereas those with low fluxes correspond to the smaller α_{irr}^0 values. In the case where the bioturbation/bioirrigation response to decreasing oxygen concentration is given by Eq. 3 (threshold function; Fig. 4), the fluxes of Mn(II) and Fe(II), as well as nitrate, decrease temporarily at around $t = 30$, following a sharp decline in the bioirrigation rate when the oxygen concentration reaches the hypoxic threshold.

In the case of phosphorus, the model simulations predict that the efflux of phosphate from the sediment will remain nearly constant in spite of declining oxygen concentrations in the overlying water (Fig. 10). The insensitivity of the phosphate flux to oxygen depletion can be explained by a simple mass balance: on decadal or longer timescales, the efflux of phosphate equals the difference between the sedimentation flux and the burial flux of phosphorus. If the sedimentation flux and the burial flux are insensitive to declining oxygen, the efflux will also be insensitive (Katsev et al. 2006b). The sedimentation flux of phosphorus is considered constant in the model, and we have no information that suggests that it varies on the timescale of interest in the St. Lawrence River Estuary. Declining oxygen concentrations also seem to have little effect on the burial flux. Burial of ferrous phosphates (represented in the model by vivianite) is relatively unaffected by oxygen depletion because a large portion of vivianite that is precipitated in the upper part of the sediment column will dissolve in the presence of hydrogen sulfide in the layers below. The same argument applies to the burial of phosphorus adsorbed to Fe(III) solids: in organic-rich sediment and in the presence of hydrogen sulfide, reactive ferric solids are reductively dissolved within the top 10 cm of the sediment (Fig. 5; Sundby et al. 2002; Anschutz et al. 1998). The decreasing size of the reactive oxidized-iron pool therefore does not have a direct effect on phosphorus burial. This is consistent with previous studies in the LSLE (Sundby et al. 1992), and with generic numerical simulations for similar sulfate-rich environments (Katsev et al. 2006b). There may be some residual phosphorus adsorbed

to the less reactive iron oxides, such as magnetite and hematite, but there is no reason to believe that this fraction of phosphorus would vary with varying oxygen in the overlying water. There is evidence that authigenic apatite (calcium phosphate) is a significant fraction of the phosphorus being permanently buried in the reduced sediment of the Gulf of St. Lawrence (Louchouart et al. 1997). Apatite precipitation was not considered in the model because it is unlikely that the rate of apatite formation and burial is affected by oxygen depletion.

Changes in sediment composition—Under conditions of constant deposition rate of Mn and Fe oxides, the efflux of dissolved Mn and Fe can increase either at the cost of decreasing the sediment inventory of dissolvable metals, or through an increase in the share of the deposited metals that is remobilized to the water column, as opposed to being permanently immobilized in the deep sediment. Since most of the Mn deposited to the sediment surface is already being returned to the water column (Fig. 7), the increase in the Mn flux (Fig. 10) has to come from the dissolution of the remaining pool of dissolvable metal (Fig. 11). Model simulations reveal that the rate at which the sedimentary pool of solid Mn is depleted depends on the recycling coefficient: The greater the efficiency of “recycling” across the sediment–water interface (higher ϵ_{Mn}), the slower is the rate of Mn depletion. In contrast to Mn, the amount of Fe that is released from the sediment is a small fraction of the total deposition flux (Fig. 7). Accordingly, a substantial increase in the efflux of dissolved Fe can be achieved with only minor changes in the iron inventory (Fig. 10), almost independently of the efficiency of iron recycling (ϵ_{Fe}).

The principal effect of decreasing oxygen on the speciation of solid iron within the sediment column is conversion of iron oxyhydroxides to sulfides (Fig. 11). The inventory of total Fe remains nearly constant. The depletion of sedimentary Fe and Mn oxides and accumulation of iron sulfides are consistent with earlier observations in seasonally hypoxic environments (Kristiansen et al. 2002).

As bottom-water oxygen concentrations decrease, the pore-water concentrations of reduced species, such as ammonium, Fe(II), and Mn(II), as well as phosphate increase, whereas the concentration of nitrate decreases. Despite an increased rate of sulfate reduction, the concentration of sulfate in the sediment pore water does not change appreciably (not shown) because the rate at which sulfate is replenished by diffusion and bioirrigation from the overlying water outpaces the rate at which it is consumed by sulfate reduction in the deep sediment.

The absence of clear temporal trends in sediment composition and benthic fluxes over the past several decades (Anschutz et al. 2000; Fig. 5) is consistent with the relatively slow rate of change predicted by our simulations for $t < 25$ yr (Figs. 10, 11). Nevertheless, our simulations suggest that sediment chemistry and elemental fluxes at the sediment–water interface will change measurably in the LSLE within the next few decades if oxygen depletion persists at the current rate.

Lagging sediment response to O₂ depletion—The oxygen depletion in the bottom water of LSLE proceeds faster than the sediment can fully respond: The decadal timescale in our simulations is shorter than the time required to reach a steady state (several hundred years). For example, for the reference parameter set, a decrease in O₂ concentration from 80 to 5 $\mu\text{mol L}^{-1}$ over a period of 75 yr increases the simulated Fe(II) flux from the sediment from 0.7 to 33 $\mu\text{mol cm}^{-2} \text{yr}^{-1}$. In contrast, the flux of Fe(II) stabilizes at 8 $\mu\text{mol cm}^{-2} \text{yr}^{-1}$ if the concentration of O₂ in the overlying water is held constant at 5 $\mu\text{mol L}^{-1}$ long enough to reach a steady state.

The critical importance of bioturbation and bioirrigation to predicting change—Our calculations show that a progressive decrease in the bottom-water oxygen concentration will increase the fluxes of reduced substances out of the sediment, deplete reactive iron and manganese oxides, and enrich the sediment in iron sulfides. In an estuarine environment, where dissolved sulfate is abundant, oxic respiration is replaced predominantly by sulfate reduction. As anoxia is approached, the concentrations and distributions of reactive phases in the sediment will change at an accelerating pace. At the long-term monitoring site at Sta. 23, these changes will become measurable within the next 20 yr. The concentration of solid-phase manganese and the partitioning of solid-phase iron between the oxidized and sulfide phases will be most affected.

The model predictions are sensitive to changes in the sedimentation flux of reactive organic carbon, the oxygen concentration at the sediment–water interface, the deposition fluxes of iron and manganese, and, most importantly, the rates and modes of bioturbation and bioirrigation. When bottom water ultimately becomes anoxic, bioturbation and bioirrigation will cease, but before that happens, decreasing bottom-water oxygen will affect the composition and functionality of the benthic community in ways that are poorly understood. Even though we are not well equipped to describe the functional dependence of bioirrigation and bioturbation on oxygen

concentration, our model results reveal that bioirrigation accounts for 40% to 99% of the solute transport between the pore water and the overlying water (Table 1). The contribution of bioirrigation is especially high for the transport of reduced species, such as Mn(II) and Fe(II), whose gradients (and therefore diffusive transport) are weak at the sediment–water interface in the presence of an oxic layer. The importance of bioirrigation is reflected in the strong dependence of model solutions on the bioirrigation coefficient α_{irr}^0 (Figs. 6, 10). The threshold-type decrease in bioirrigation in response to oxygen depletion (Eq. 3) temporarily lowers the Mn and Fe fluxes at $\sim t = 30$ (Fig. 10). The decrease in bioturbation has a different effect. As the rate of mixing decreases, reduction of oxidized phases takes place progressively closer to the sediment–water interface, and the diffusive fluxes of Fe and Mn from the sediment increase. The shallowing of the redox boundary is responsible for increasing the effluxes of reduced elements during the last stages of oxygen depletion (Fig. 10). This modeling exercise thus illustrates the importance of relative responses of bioirrigator vs. bioturbator communities.

The uncertainties in the projected flux values reported in Fig. 10 are large. For the flux of Mn(II), the uncertainty is as high as 80% in the vicinity of anoxia. The lack of understanding of how the benthic community responds to slowly decreasing oxygen availability is the single most important obstacle to predicting the timing and magnitude of changes in sediment composition and fluxes. Faunal succession stages along a spatial oxygen gradient (Pearson and Rosenberg 1978; Rhoads et al. 1978; Rosenberg 2001) suggest that benthic diversity and bioturbation depth decrease gradually with decreasing oxygen availability, but it is not clear how well these conceptual models describe the benthic responses to temporal changes in oxygen levels, nor is it clear how changes in the benthic communities affect the intensities and modes of bioturbation and bioirrigation. A large body of evidence supports the notion that drastic changes in benthic diversity result when the oxygen concentration falls below a certain threshold, but the value of this threshold is still the subject of debate. Low oxygen concentrations do not necessarily eliminate bioturbation and bioirrigation completely, since actively bioturbating animals can be present in environments with permanently low dissolved oxygen levels ($< 3 \mu\text{mol L}^{-1}$) (Levin et al. 2003). It is thus possible that an area of the seafloor affected by low oxygen levels can be colonized, given sufficient time, by species such as nematode or tubificid worms that are tolerant to the low oxygen conditions. In addition, variations in the sediment bioturbation and bioirrigation activity can affect the rate of organic carbon decomposition (Kristensen 2000), which is in itself an important control on sediment diagenesis.

References

- ALLER, R. C. 1994. The sedimentary Mn cycle in Long Island Sound—its role as intermediate oxidant and the influence of bioturbation, O₂, and C(Org) flux on diagenetic reaction balances. *J. Mar. Res.* **52**: 259–295.

- ANDERSON, L. 1979. Simultaneous spectrophotometric determination of nitrite and nitrate by flow injection analysis. *Anal. Chim. Acta* **110**: 123–128.
- ANSCHUTZ, P., B. SUNDBY, L. LEFRANCOIS, G. W. LUTHER III, AND A. MUCCI. 2000. Interactions between metal oxides and species of nitrogen and iodine in bioturbated marine sediments. *Geochim. Cosmochim. Acta* **64**: 2751–2763.
- , S. ZHONG, B. SUNDBY, A. MUCCI, AND C. GOBEIL. 1998. Burial efficiency of phosphorus and the geochemistry of iron in continental margin sediments. *Limnol. Oceanogr.* **43**: 53–64.
- BARNETT, P. R. O., J. WATSON, AND D. CONNELLY. 1984. A multiple corer for taking virtually undisturbed samples from shelf, bathyal and abyssal sediments. *Oceanol. Acta* **7**: 399–408.
- BELZILE, N. 1987. Étude géochimique de l'arsenic et du sélénium dans les sédiments du chenal laurentien. Ph.D. thesis, Université du Québec à Rimouski.
- BENOIT, P., Y. GRATTON, AND A. MUCCI. 2006. Modeling of dissolved oxygen levels in the bottom waters of the Lower St. Lawrence Estuary: Coupling of benthic and pelagic processes. *Mar. Chem.* **102**: 13–32.
- BERG, P., S. RYSGAARD, AND B. THAMDRUP. 2003. Dynamic modeling of early diagenesis and nutrient cycling. A case study in an Arctic marine sediment. *Am. J. Sci.* **303**: 905–955.
- BOURGALT, D., AND V. KOUTITONSKY. 1999. Real-time monitoring of the freshwater discharge at the head of the St. Lawrence Estuary. *Atmos. Ocean* **37**: 203–220.
- BURDIGE, D. J. 2006. *Geochemistry of marine sediments*. Princeton Univ. Press.
- DIAZ, R. J., AND R. ROSENBERG. 1995. Marine benthic hypoxia: A review of its ecological effects and the behavioural responses of benthic macrofauna. *Oceanogr. Mar. Biol. Ann. Rev.* **33**: 245–303.
- EDENBORN, H. M., N. SILVERBERG, A. MUCCI, AND B. SUNDBY. 1987. Sulfate reduction in deep coastal marine sediments. *Mar. Chem.* **21**: 329–345.
- EPPING, E. H. G., AND W. HELDER. 1997. Oxygen budgets calculated from in situ oxygen micropfiles for Northern Adriatic sediments. *Cont. Shelf Res.* **17**: 1737–1764.
- FORSTER, S., G. GRAF, J. KITLAR, AND M. POWILLEIT. 1995. Effects of bioturbation in oxic and hypoxic conditions—a microcosm experiment with a North-Sea sediment community. *Mar. Ecol. Prog. Ser.* **116**: 153–161.
- FOSSING, H., P. BERG, B. THAMDRUP, S. RYSGAARD, H. M. SORENSEN, AND K. NIELSEN. 2004. A model set-up for an oxygen and nutrient flux model for Aarhus Bay (Denmark). National Environmental Research Institute (NERI), University of Aarhus, Technical Report 483.
- GILBERT, D., B. SUNDBY, C. GOBEIL, A. MUCCI, AND G.-H. TREMBLAY. 2005. A seventy-two year record of diminishing deep-water oxygen in the St. Lawrence Estuary: The north-west Atlantic connection. *Limnol. Oceanogr.* **50**: 1654–1666.
- GLUD, R. N., J. K. GUNDERSEN, B. B. JORGENSEN, N. P. REVSBECH, AND H. D. SCHULZ. 1994. Diffusive and total oxygen uptake of deep-sea sediments in the eastern South Atlantic Ocean: In situ and laboratory measurements. *Deep-Sea Res. I* **41**: 1767–1788.
- GOBEIL, C., R. W. MACDONALD, AND B. SUNDBY. 1997. Diagenetic separation of Cd and Mn in suboxic continental margin sediments. *Geochim. Cosmochim. Acta* **61**: 4647–4654.
- , AND N. SILVERBERG. 1989. Early diagenesis of lead in Laurentian Trough sediments. *Geochim. Cosmochim. Acta* **53**: 1889–1895.
- HULTH, S., T. H. BLACKBURN, AND P. O. J. HALL. 1994. Arctic sediment (Svalbard): Consumption and microdistribution of oxygen. *Mar. Chem.* **46**: 293–316.
- JUNG, M., J. ILMBERGER, A. MANGINI, AND K.-C. EMEIS. 1997. Why some Mediterranean sapropels survived burn-down (and others did not). *Mar. Geol.* **141**: 51–60.
- KATSEV, S., D. G. RANCOURT, AND I. L'HEUREUX. 2004. dSED: A database tool for modeling sediment early diagenesis. *Comp. Geosci.* **30**: 959–967.
- , B. SUNDBY, AND A. MUCCI. 2006a. Modeling vertical excursions of the redox boundary in sediments: Application to deep basins of the Arctic Ocean. *Limnol. Oceanogr.* **51**: 1581–1593.
- , I. TSANDEV, I. L'HEUREUX, AND D. G. RANCOURT. 2006b. Factors controlling long term phosphorus efflux in lake sediments: Exploratory reaction-transport modeling. *Chem. Geol.* **234**: 127–147.
- KRISTENSEN, E. 2000. Organic matter diagenesis at the oxic/anoxic interface in coastal marine sediments, with emphasis on the role of burrowing animals. *Hydrobiologia* **426**: 1–24.
- KRISTIANSEN, K. D., E. KRISTENSEN, AND E. M. JENSEN. 2002. The influence of water column hypoxia on the behaviour of manganese and iron in sandy coastal marine sediment. *Estuar. Coast. Shelf Sci.* **55**: 645–654.
- LARSEN, O., D. POSTMA, AND R. JAKOBSEN. 2006. The reactivity of iron oxides towards reductive dissolution with ascorbic acid in a shallow sandy aquifer (Rømø, Denmark). *Geochim. Cosmochim. Acta* **70**: 4827–4835.
- LAVIGNE, C., S. K. JUNIPER, AND N. SILVERBERG. 1997. Spatio-temporal variability in benthic microbial activity and particle flux in the Laurentian Trough. *Deep-Sea Res. I* **44**: 1793–1813.
- LEVIN, L. A., A. E. RATHBURN, D. GUTIERREZ, P. MUNOZ, AND A. SHANKLE. 2003. Bioturbation by symbiont-bearing annelids in near-anoxic sediments: Implications for biofacies models and paleo-oxygen assessments. *Palaeogeog. Palaeocl.* **199**: 129–140.
- LOUCHOUART, P., M. LUCOTTE, E. DUCHEMIN, AND A. DE VERNAL. 1997. Early diagenetic processes in recent sediments of the Gulf of St-Lawrence: phosphorus, carbon and iron burial rates. *Mar. Geol.* **139**: 181–200.
- MEILE, C., P. BERG, P. VAN CAPPELLEN, AND K. TUNCAY. 2005. Solute-specific pore water irrigation: Implications for chemical cycling in early diagenesis. *J. Mar. Res.* **63**: 601–621.
- MEYSMAN, F. J. R., B. P. BOUDREAU, AND J. J. MIDDELBURG. 2005. Modeling reactive transport in sediments subject to bioturbation and compaction. *Geochim. Cosmochim. Acta* **69**: 3601–3617.
- MILLERO, F. J., S. SOTOLONGO, AND M. IZAGUIRE. 1987. The oxidation kinetics of Fe(II) in seawater. *Geochim. Cosmochim. Acta* **51**: 793–801.
- MORGAN, J. J. 2005. Kinetics of reaction between O₂ and Mn(II) species in aqueous solutions. *Geochim. Cosmochim. Acta* **69**: 35–48.
- MORSE, J. W., AND P. M. ELDRIDGE. 2007. A non-steady-state diagenetic model for changes in sediment biogeochemistry in response to seasonally hypoxic/anoxic conditions in the “dead zone” of the Louisiana shelf. *Mar. Chem.* **106**: 239–255. doi:10.1016/j.marchem.2006.02.003.
- MURPHY, J., AND J. P. RILEY. 1962. A modified single solution method for determination of phosphate in natural waters. *Anal. Chim. Acta* **26**: 31.
- PEARSON, T. H., AND R. ROSENBERG. 1978. Macrobenthic succession in relation to organic enrichment and pollution of the marine environment. *Oceanogr. Mar. Biol. Ann. Rev.* **16**: 229–311.
- PETRIE, B., K. DRINKWATER, A. SANDSTRÖM, R. PETTIPAS, D. GREGORY, D. GILBERT, AND P. SEKHON. 1996. Temperature, salinity and sigma-t atlas for the Gulf of St. Lawrence. Canadian Technical Report of Hydrography and Ocean Sciences 178.

- REICHERT, P., M. SCHERVISH, AND M. J. SMALL. 2002. An efficient sampling technique for Bayesian inference with computationally demanding models. *Technometrics* **44**: 318–427.
- REVSBECH, N. P., B. B. JORGENSEN, AND T. H. BLACKBURN. 1980. Oxygen in the sea bottom measured with a microelectrode. *Science* **207**: 1355–1356.
- RHOADS, D. C., P. L. MCCALL, AND J. Y. YINGST. 1978. The ecology of seafloor disturbance. *Am. Sci.* **198**: 577–586.
- RICHARD, L.-F. 1995. Comparaison des comportements géochimiques du phosphore et de l'arsenic dans le fjord du Saguenay et l'estuaire du St-Laurent. M.Sc. thesis, Université du Québec à Montréal.
- RITTER, C., AND P. A. MONTAGNA. 1999. Seasonal hypoxia and models of benthic response in a Texas bay. *Estuaries* **22**: 7–20.
- ROSENBERG, R. 2001. Marine benthic faunal successional stages and related sedimentary activity. *Sci. Mar.* **65**: 107–119.
- SAYLES, F. L., W. R. MARTIN, AND W. G. DEUSER. 1994. Response of benthic oxygen-demand to particulate organic-carbon supply in the deep-sea near Bermuda. *Nature* **371**: 686–689.
- SELL, K. S., AND J. W. MORSE. 2006. Dissolved Fe²⁺ and H₂S behavior in sediments seasonally overlain by hypoxic-to-anoxic waters as determined by CSV microelectrodes. *Aquat. Geochem.* **12**: 179–198.
- SILVERBERG, N., J. BAKKER, H. M. EDENBORN, AND B. SUNDBY. 1987. Oxygen profiles and organic-carbon fluxes in Laurentian Trough sediments. *Netherlands J. Sea Res.* **21**: 95–105.
- , J.-M. GAGNON, AND K. LEE. 1995. A benthic mesocosm facility for maintaining soft-bottom sediments. *Netherlands J. Sea Res.* **34**: 289–302.
- , AND B. SUNDBY. 1990. Sediment-water interaction and early diagenesis in the Laurentian Trough, p. 202–238. *In* M. El-Sabh and N. Silverberg [eds.], *Coastal and Marine Studies*, v. 39. Springer-Verlag.
- , B. SUNDBY, A. MUCCI, S. ZHONG, T. ARAKAKI, P. HALL, A. LANDEN, AND A. TENBERG. 2000. Remineralization of organic carbon in Eastern Canadian margin sediments. *Deep-Sea Res.* **47**: 699–731.
- SOETAERT, K., P. M. J. HERMAN, AND J. J. MIDDELBURG. 1996. Dynamic response of deep-sea sediments to seasonal variations: A model. *Limnol. Oceanogr.* **41**: 1651–1668.
- , J. J. MIDDELBURG, P. M. J. HERMAN, AND K. BUIS. 2000. On the coupling of benthic and pelagic biogeochemical models. *Earth-Sci. Rev.* **51**: 173–201.
- STOOKEY, L. L. 1970. Ferrozine—a new spectrophotometric reagent for iron. *Anal. Chem.* **42**: 779–781.
- SUNDBY, B., C. GOBEIL, N. SILVERBERG, AND A. MUCCI. 1992. The phosphorus cycle in coastal marine sediments. *Limnol. Oceanogr.* **37**: 1129–1145.
- , AND N. SILVERBERG. 1985. Manganese fluxes in the benthic boundary layer. *Limnol. Oceanogr.* **30**: 372–381.
- , N. SILVERBERG, AND R. CHESSELET. 1981. Pathways of manganese in an open estuarine system. *Geochim. Cosmochim. Acta* **45**: 293–307.
- THAMDRUP, B., H. FOSSING, AND B. B. JORGENSEN. 1994. Manganese, iron, and sulfur cycling in a coastal marine sediment, Aarhus Bay, Denmark. *Geochim. Cosmochim. Acta* **58**: 5115–5129.
- THIBODEAU, B., A. DE VERNAL, AND A. MUCCI. 2006. Recent eutrophication and consequent hypoxia in the bottom waters of the Lower St. Lawrence Estuary: Micropaleontological and geochemical evidence. *Mar. Geol.* **231**: 37–50.
- THOMSON, J., N. C. HIGGS, AND S. COLLEY. 1996. Diagenetic redistributions of redox-sensitive elements in northeast Atlantic glacial/interglacial transition sediments. *Earth Planet. Sci. Lett.* **139**: 365–377.
- YEATS, P. A. 1988. Nutrients, p. 29–48. *In* P. M. Strain [ed.], *Chemical oceanography in the Gulf of St. Lawrence*. *Can. Bull. Fish. Aquat. Sci.* 220.

Received: 25 January 2007

Accepted: 7 July 2007

Amended: 23 July 2007